

Renewable Resource-Based Hybrid Crosslinker for Sustainable Industrial Coatings

Dinesh Balgude and Anagha Sabnis*

Department of Polymer and Surface Engineering, Institute of Chemical Technology, Nathalal Parekh Marg, Matunga (E), Mumbai-400019, Maharashtra, India

Received April 12, 2014; Accepted July 17, 2014

ABSTRACT: Renewable resource-based hybrid crosslinker was successfully synthesized via sol-gel technology. The synthesis involved malenization of Cashew Nut Shell Liquid (CNSL) followed by its silane modification and subsequent hydrolysis and condensation with tetraethyl orthosilicate (TEOS). The synthesized crosslinker was characterized by spectroscopic analysis (FT-IR, ¹H-NMR, ¹³C-NMR and ²⁹Si-NMR) for structural elucidation. The crosslinker was further formulated in a conventional stoving system. Fully-cured coatings were obtained after stoving at 120°C for ½ hr and were then evaluated for physical, mechanical, chemical, optical, accelerated weathering, electrochemical and morphological properties. The incorporation of hybrid crosslinker in a conventional stoving system was observed to improve overall coating properties. The excellent properties can be attributed to the combination of an aliphatic chain of CNSL and siloxane (-Si-O-Si-) moieties within the coating, resulting in good balance of flexible and dense structure which would take care of load distribution properties and penetration of corrosive chemicals through coatings.

KEYWORDS: CNSL, hybrid crosslinker, performance properties, renewable resource, sol-gel

1 INTRODUCTION

Alkyd-melamine chemistry is one of the widely used resin systems in various coating applications, such as industrial coatings, product finish coatings, etc., with moderate performance properties. These binders are mainly derived from petroleum-based feedstocks. Though exhibiting desired coating properties, the utilization of petroleum feedstocks has been vanishing due to stringent economic and environmental concerns [1,2]. In this regard, the exploration of renewable resources by various chemical modifications, such as for resin synthesis, has been a well-accepted approach in the last decades [3–9]. The use of renewable resources is mainly due to the fact that these materials are eco-friendly, user friendly and economical, and thereby provide a three-fold solution to various concerns of the modern coating industry [10]. Till now a number of renewable resources have been explored in resin synthesis, some of them being oils, rosin, tannin, lignin, polysaccharide (sugar alcohols, starch, polycarboxylic

acids), etc. [11–15]. However, there exist compounds like Cashew Nut Shell Liquid (CNSL), which can be used as possible substitutes for petroleum-based materials due to their availability, sustainability, cost effectiveness, and reactive functionalities.

A waste agricultural byproduct of the cashew nut industry, CNSL contains a number of useful phenolic derivatives with meta substituted long-chain saturated/unsaturated hydrocarbons. These reactive functionalities make it suitable for a number of polymerization reactions through addition as well as condensation mechanisms. On this basis, it was used in a number of industrial applications like laminating resins, adhesives, ion-exchange resins, paints and coatings, lacquers, hybrid materials, waterproofing agents, surface active agents, color and dyes, coupling agents, corrosion inhibitors, etc. [16].

Nowadays, a number of advanced coating technologies have come on the market to enhance the performance properties of conventional coatings, some of them being self-healing coatings, conductive coatings, sol-gel technology, etc. [17–19]. Among all the technologies, sol-gel technology has been widely used due to a number of advantages it possesses such as room temperature synthesis, chemical inertness, high oxidation and abrasion resistance, excellent

*Corresponding author: as.sabnis@ictmumbai.edu.in

DOI: 10.7569/JRM.2014.634115

thermal stability, excellent barrier and mechanical properties, very low health hazard, etc. [20]. In our previous paper we thoroughly reported the various types of hybrid coatings, their basic chemistries and synthesis, their interaction with metal and subsequent coating, as well as current developments, etc., as far as metal protection is concerned [21]. Organic-inorganic hybrid coatings offer an excellent adhesion to metals as well as to the subsequent coat via strong covalent bond and a three-dimensional network of siloxane ($-\text{Si}-\text{O}-\text{Si}-$) linkages, which help to retard the penetration of corrosive medium through the coating.

This proposed work deals with the development of hybrid crosslinker from modified renewable resource via sol-gel technology and its application in a conventional stoving system. The combination of biobased material and sol-gel technology serves the purpose of sustainability with enhanced performance properties.

2 MATERIALS

Cashew nut shell liquid (NC-700) was procured from Cardolite Corporation, Mangalore; 3-glycidyloxypropyl trimethoxysilane (GPTMS) and Tetraethyl orthosilicate (TEOS) were obtained from Wacker Silicones, Mumbai. Maleic anhydride, anhydrous sodium sulphate (Na_2SO_4), glacial acetic acid (GAA), methanol, xylene, p-toluene sulfonic acid (p-TSA), and triethylamine (TEA) were purchased from SD Fine-Chem Ltd., Mumbai. Short oil alkyd (Replakyd-526) was procured from Resins and Plastics Ltd., Mumbai. Hexabutoxymethylmelamine (HBMM) was procured from Shalimar Paints Ltd, Nashik, India.

3 EXPERIMENTAL

3.1 Synthesis of Malenized CNSL-Based Hybrid Precursor (MCHP)

The synthesis of MCHP involved malenization of CNSL and subsequent hydrolysis of malenized CNSL followed by GPTMS modification. At first, malenization of CNSL was carried out in a molar ratio of 2.2:1 (maleic anhydride: CNSL) in a 4-neck round-bottom flask fitted with thermometer pocket, water condenser, dry nitrogen inlet and was mixed using a motor-driven stirrer at elevated temperature (180–200°C) for 4½ hrs. Conventionally, malenization reaction proceeds radically or thermally. However, undesired currying reaction unavoidably occurs, resulting in gelation of the reaction mixture. The reaction mixture was charged with nitrogen

containing solvent such as n-methyl-2-pyrrolidone (2 wt%) to process the malenization reaction without gelation [22]. During malenization reaction, maleic anhydride is grafted on to the unsaturated chain of CNSL via Diels-Alder/Ene mechanism [23]. This mechanism involved the transfer of active proton (proton from methylene [$-\text{HC}=\text{CH}-$] group) of maleic anhydride to the reactive double bond (C_8 and C_{11}) of CNSL, resulting in grafting of maleic anhydride on CNSL with shifting of double bond on CNSL molecule. After the malenization reaction, hydration was carried out by boiling malenized CNSL in water for 1 hr. Hydration results in the opening of the anhydride rings. The excess water was distilled off under reduced pressure followed by passing the product over anhydrous sodium sulphate to remove the water traces. The purified malenized CNSL was then evaluated for its Acid value and it was observed to be 230 mg KOH/ gm.

Silane-modified malenized CNSL was then synthesized by reacting hydrolyzed malenized CNSL with GPTMS at 60–70°C for 4 hrs under magnetic stirring (molar ratio of GPTMS / malenized CNSL = 0.2/1). Triethylamine (0.2 wt%) was used to catalyze the reaction. After completion of the reaction, product was analyzed for its Acid value. Figure 1 shows a schematic representation of malenization of CNSL followed by its hybridization via sol-gel technology.

3.2 Preparation of MCHP-Based Primary Sol

The primary sol was then synthesized by hydrolyzing the mixture of TEOS and MCHP (molar ratio of $\text{H}_2\text{O}/\text{Si} = 15:1$) along with methanol at room temperature (30°C) under magnetic stirring at a rate of 150 rpm for 24 hrs. TEOS and methanol were added with respect to GPTMS content in MCHP (molar ratio of TEOS/GPTMS/ Methanol = 1:2:2 respectively). An electronic pH meter (Digital pH Meter Model: pH 600, Sigma Instruments) was used to monitor the pH of solution, which was maintained in the range of 2–4 using 0.05 M Glacial acetic acid (GAA) [24]. The GAA was added with respect to total reaction solids (1 wt% of reaction solids).

3.3 Coating Preparation

The synthesized precursor was further used as a partial crosslinker in a conventional alkyd-HBMM-based stoving system. The curing ratio of alkyd to HBMM was set at 70:30 wt% respectively. The coating solutions were formulated by replacing HBMM with primary sol at 30 and 50 wt%. For comparative

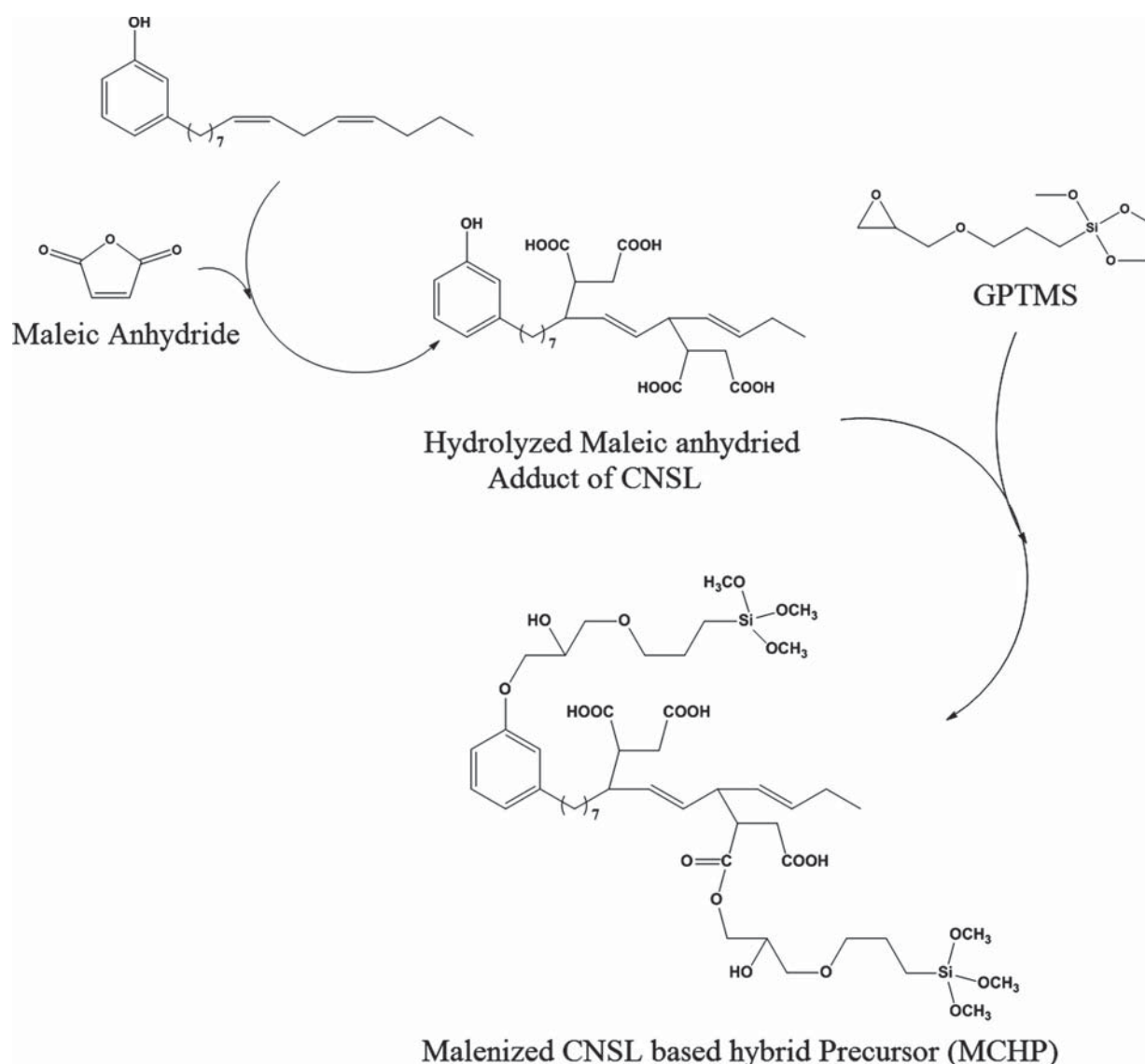


Figure 1 Synthesis of Malenized CNSL-based hybrid precursor.

study, the neat coating solution was also applied. The coatings were designated as HC_0, HC_30 and HC_50, where HC stands for hybrid coatings while the number represents weight percentage replacement of HBMM with MCHP.

3.4 Surface Preparation, Coating Deposition and Its Curing

Mild steel panels (2×3 square inches) were manually cleaned before application. Cleaning involved degreasing, hand scrubbing using emery paper (120 no.), followed by methanol cleaning. The application viscosity of all the coating solutions was maintained

at 40% nonvolatile matter (%NVM) using a mixture of xylene and methyl ethyl ketone in 90:10 wt% ratios. The coating solutions were then applied onto prepared substrates by conventional airless spray application according to ASTM D 4708-99. The coated substrates were allowed to air dry for 10 minutes and were then placed in an air circulating oven to cure at 120°C for $\frac{1}{2}$ hr. Typical dry-film thickness of coatings was observed to be in the range of 50–60 microns. The completely cured panels were evaluated for mechanical properties, chemical and solvent resistance properties, hydrolytic stability, optical properties, anti-corrosive properties, electrochemical properties and SEM/EDAX analysis as per ASTM standards.

4. METHODS AND MEASUREMENT

The malenization of CNSL and subsequent hydrolysis were characterized for presence of functional groups by Fourier transform infrared spectroscopy (FTIR) in the spectra range of $500\text{--}4000\text{cm}^{-1}$ on Perkin-Elmer Spectrum 100 Instrument as per ASTM E-1252. Further, the prepared primary sol was characterized by nuclear magnetic resonance spectroscopy ($^1\text{H-NMR}$, $^{13}\text{C-NMR}$ and $^{29}\text{Si-NMR}$) for structural elucidation on Bruker Biospin (Avance AV500WB, Germany) spectrometer at 400 MHz using deuterated chloroform as solvent and tetramethylsilane (TMS) as an internal standard.

Applied coatings were evaluated for adhesion properties by cross-cut adhesion according to ASTM D-3359. Pencil hardness of the coating was measured on a hardness tester according to ASTM D-3363. Flexibility and load distribution property (impact resistance) of the coatings were tested by conical mandrel and impact tester as per ASTM D-522 and ASTM D-2794 respectively. Impact resistance was measured on the impact tester with maximum height of 60 cm and load of 1.36 kg. The chemical and solvent resistance of the coatings were evaluated by immersing the coated panels in 5% HCl, 5% NaOH, methanol and xylene according to ASTM D-1308 respectively. The hydrolytic stability of the coatings was evaluated as per ASTM-B-1308 method. The coated panel was immersed in boiling water for 4 hours. After chemical, solvent resistance and hydrolytic stability tests, coated panels were evaluated for degree of adhesion and visual inspection of blisters and cracks, if any.

The cured coatings were further evaluated for salt spray resistance (ASTM B-117) and UV resistance (ASTM-G53) to investigate the anti-corrosive performance and outdoor weatherability of the coated panels respectively. The UV resistance was synchronized with the color spectrophotometer (COLOR-EYE 7000) to evaluate the color values, % variation in Yellowness index and ΔE values after the testing.

The electrochemical properties of the coatings were evaluated by impedance spectroscopic analysis on VersaSTAT-3 instrument (AMETEK, Princeton Applied Research, Oak Ridge, TN, USA). The electrochemical studies involved 3-electrode systems namely, saturated calomel electrode, a platinum electrode and a coated panel acting as reference, counter and working electrode respectively. The electrode surface area exposed to testing solution (3.5 wt% NaCl) was 7 cm^2 in all cases. All the electrochemical measurements were carried out at room temperature (32°C) in 3.5 wt% NaCl solution.

Surface morphology and elemental distribution across the coating were characterized by scanning electron microscope (SEM) and energy

dispersive spectroscopy (EDAX) using Quanta 200 SEM instrument (FEI Company, USA).

5. RESULTS AND DISCUSSION

5.1 Synthesis

5.1.1 FTIR Analysis

The malenization of CNSL and subsequent hydrolysis was confirmed by FTIR and compared with CNSL spectrum. The appearance of transmission band at 1715 and 1740 cm^{-1} (in Figure 2) corresponding to C=O stretching from carboxylic (-COOH) group after anhydride ring opening is due to hydrolysis which was observed to be absent in CNSL spectrum [25]. Figure 3 shows the FTIR spectra of GPTMS modified hydrolyzed malenized CNSL and neat GPTMS. The disappearance of peak at 909 cm^{-1} due to C-O stretching of oxirane group of GPTMS confirmed the complete utilization of oxirane group by acidic group of malenized CNSL.

Figure 4 shows the FTIR spectra of CNSL-based hybrid coating containing various percentages of MCHP. The graph shows an increase in intensity of peaks at 550 cm^{-1} , 1017 cm^{-1} , 1084 cm^{-1} , and 1261 cm^{-1} , which corresponds to -Si-O-Fe-, -Si-O-Si-, -Si-O-CH₃ and Si-C [26–28] respectively on increasing the MCHP concentration. The increased intensity of Si-O stretching in the above-mentioned linkages indicates that the condensation reactions occurred between silanol and metal substrate lead to the formation of strong covalent bond at metal coating interface. The increased silicon-oxygen-metal (-Si-O-Fe-) linkages improved the adhesive forces at the metal coating interface, while increased siloxane linkages (-Si-O-Si-) provided

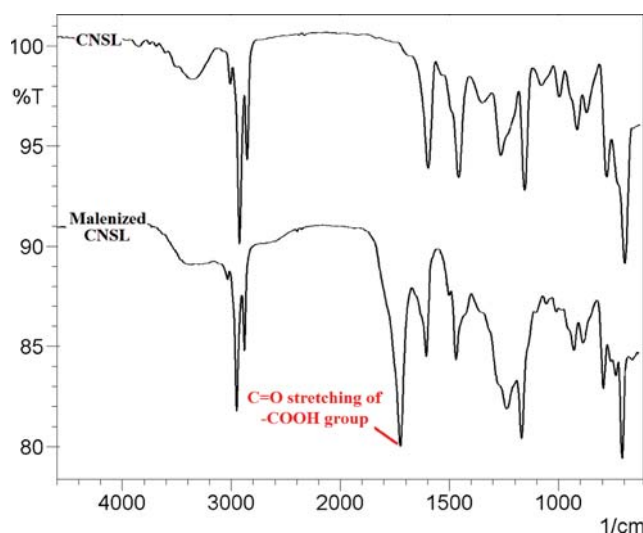


Figure 2 FTIR spectra of CNSL and Malenized CNSL (after hydrolysis).

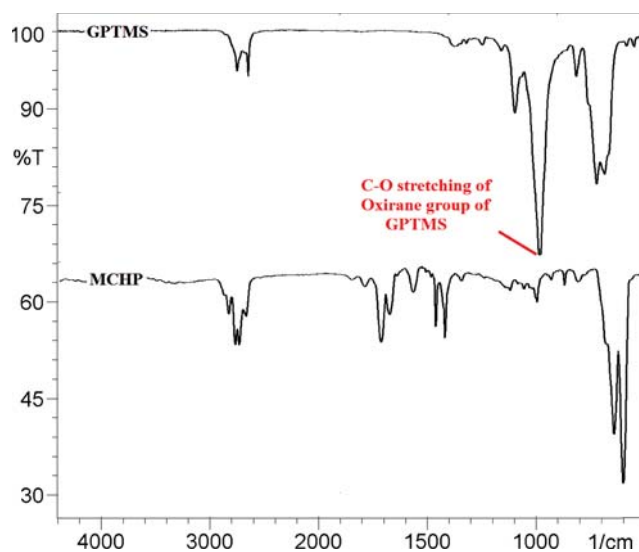


Figure 3 FTIR spectra of GPTMS and GPTMS modified Malenized CNSL (MCHP).

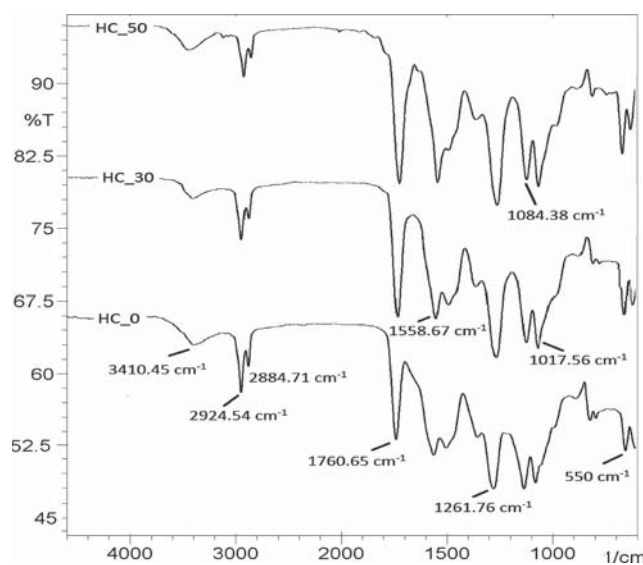


Figure 4 FTIR spectra of CNSL-based hybrid coatings containing various percentages of MCHP.

enhanced barrier layer for the ingress of aggressive chemicals and hence improved corrosion protection.

Frequency at 3460 cm^{-1} denoted the existence of OH groups. The sharp peaks at 2924 cm^{-1} and around 2884 cm^{-1} are due to $-\text{CH}_3$ symmetric stretching and $\text{O}-\text{CH}_3$ asymmetric stretching vibrations. The absorption band at 1730 cm^{-1} corresponds to $-\text{C}=\text{O}$ stretching of the carboxyl group. The significant decrease in peak intensity at 1558 cm^{-1} which corresponds to $-\text{C}-\text{N}$ stretching of HBMM, confirmed the replacement of HBMM by MCHP, while the sharp peak at 1261 cm^{-1} is attributed to $\text{Si}-\text{C}$ symmetric bending of $\text{Si}-\text{CH}_3$ group respectively.

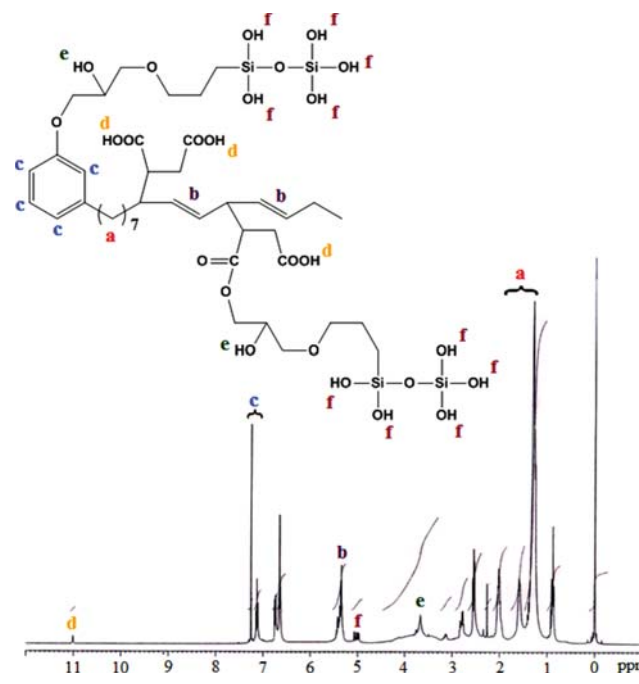


Figure 5 ^1H -NMR spectra of primary sol.

5.1.2 NMR Analysis

The prepared primary sol was characterized by NMR spectroscopy. The representative ^1H -NMR spectrum of prepared primary sol (Figure 5) shows chemical shift (ppm) at 1.3–1.6, 5.48 and 7.1–7.3, which indicated the proton from $-\text{CH}_2-$, $-\text{CH}-$, and C_6H_6 respectively. While, the signals at 11, 3.58 and 5 ppm representing proton from carboxylic, alcoholic and silanol groups respectively [29], confirmed the malenization of CNSL followed by GPTMS modification.

Also, ^{13}C -NMR spectrum of prepared primary sol (Figure 6) shows peaks for carbon from $-\text{CH}_2-$, $-\text{CH}-$ of aliphatic unsaturation and from aromatic ring at 29.3–36 ppm, 132.4–133.1 ppm, 111.6–129.1 and 142.3–157.2 ppm respectively [29]. This represents the structure of CNSL having benzene ring with unsaturated aliphatic chain, while chemical shift (ppm) at 172.0–177.3, 42.3–42.6 and 70.5–71.2 represents carbon from $-\text{COO}$, $-\text{CH}-$ from maleic anhydride and $-\text{CH}-$ attached to free hydroxyl, which confirmed the malenization and subsequent GPTMS modification of CNSL.

The peak assignments in ^{29}Si -NMR spectra of primary sols are described as previously reported by Glaser *et al.* for organically modified silanes [30]. The spectra (as shown in Figure 7) shows distinct peaks for the silica network units at -49.5 to -50.5 ppm [T^1], -56.5 to -59.3 ppm [T^2], and 65.8 to -69.9 ppm [T^3], which corresponds to $\text{R}-\text{Si}(\text{OR})_2(\text{O})_1$, $\text{R}-\text{Si}(\text{OR})(\text{O})_2$, $\text{R}-\text{Si}(\text{O})_3$, respectively. Also, the spectra shows some low intensity peaks at -93.7 to -94.5 ppm [Q^2], -102.4

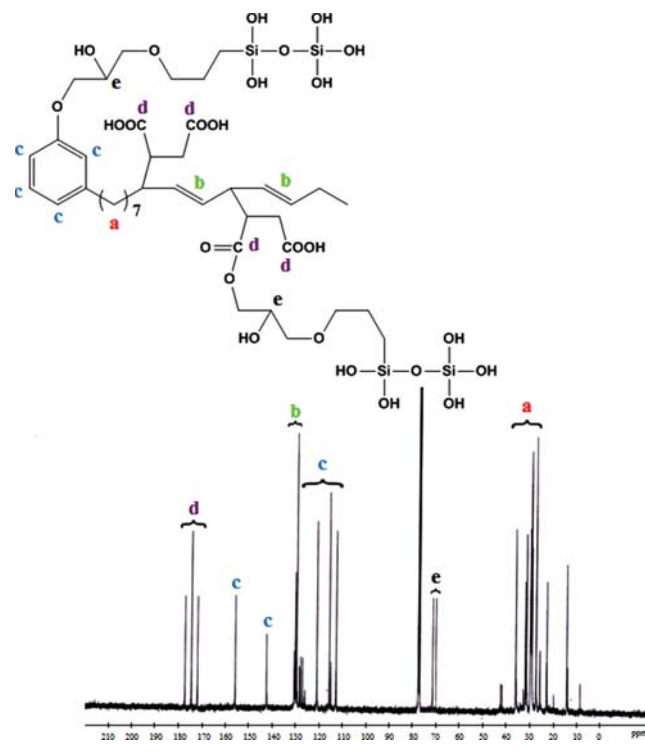


Figure 6 ^{13}C -NMR spectra of primary sol.

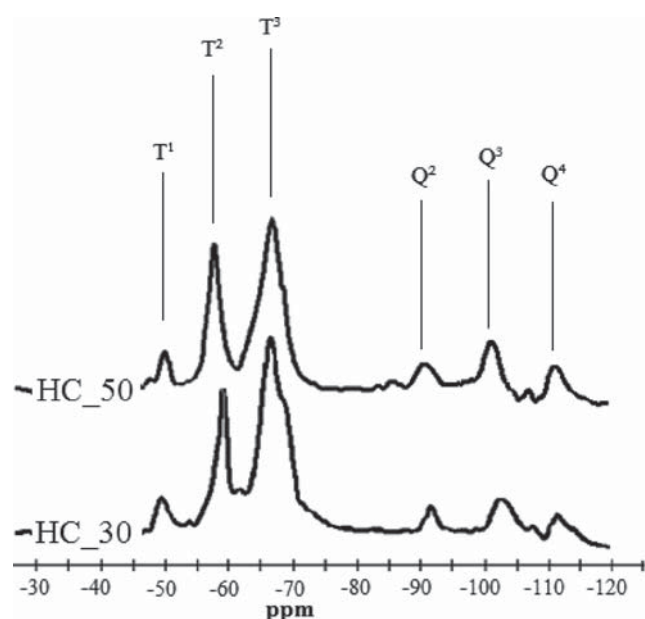


Figure 7 ^{29}Si -NMR spectra of coating formulations.

to -103.3 ppm [Q^3], and -111.6 to -113.7 ppm [Q^4] attributed to $\text{Si}(\text{OSi})_2(\text{OH})_2$, $\text{Si}(\text{OSi})_3(\text{OH})$, and $\text{Si}(\text{OSi})_4$, respectively. This could be due to formation of mono-, di-, tri- or tetra-siloxane linkages in the matrix. Thus, ^{29}Si -NMR measurements confirmed the formation of a dense siloxane network evident from increasing peak ratios of T^2/T^3 and Q^2/Q^3 on increasing MCHP

content (Figure 7). This indicated the enhancement in the degree of condensation in the sol. The increased degree of condensation has led to the formation of a higher reticulated network of TEOS and GPTMS into the hybrid silane matrix.

5.1.3 Chemical Analysis

Acid value is a measure of carboxyl content present in the given molecular structure as per ASTM D-1980. The GPTMS modification of malenized CNSL was characterized by measuring the Acid value of reaction mixture before the start of reaction and after completion of reaction. The Acid value of reaction mixture containing Malenized CNSL and GPTMS was observed to be decreased from the initial 192 to 154 mg of KOH/gm at the end of GPTMS modification. This confirmed the consumption of acidic proton to open the oxirane group of GPTMS.

5.2 Coating Properties

5.2.1 Optical Property

Optical property of the coatings was evaluated using a digital gloss meter at 60° . There was no significant difference observed in the gloss values of all the systems. Table 1 shows the gloss value for all the formulations.

5.2.2 Mechanical Properties

The cross hatch adhesion as well as flexibility were observed to be excellent in all the coatings irrespective of the percentage of GPTMS modification. The presence of polar functional groups (such as carboxyl and hydroxyl) of MCHP-based primary sol would contribute to the strong adhesive forces to the metal substrate, while long methylene linkages of CNSL would take care of any increased crystallinity by increasing the content of MCHP-based hybrid sol, thus contributing to excellent flexibility of the coatings. However, the pencil hardness was observed to be increased with increasing percentage of hybrid sol. This could be due to increasing percentage of MCHP resulting in a dense crosslinked polymeric network leading to increased surface hardness of the cured coatings.

The load distribution property of the coatings was evaluated by falling ball impact method and it was observed to be increased with increasing concentration of hybrid precursor. The increased number of methylene linkages on increasing the percentage of hybrid sol was responsible for imparting very good flexibility to the systems. The excellent flexibility of the coating was adequate to provide excellent load distribution property on impact without any crack.

Table 1 General coating properties of CNSL-based hybrid coatings.

Properties	HC_0 (Neat)	HC_30	HC_50
Dry film thickness (<i>ASTM D-1186</i>)	52-56 μm	55-60 μm	53-59 μm
Gloss (60°) (<i>ASTM D-523</i>)	99-103	102-105	100-103
Cross-hatch Adhesion (<i>ASTM D-3359</i>)			
Primary (at 0 hrs of salt spray exposure)	5B	5B	5B
Secondary (after 250 hrs of salt spray exposure)	3B	4B	5B
Flexibility (Conical Mandrel, 3mm diameter) (<i>ASTM D-522</i>)	No fracture	No fracture	No fracture
Impact (inch-pound, weight of block = 1.36 kg) (<i>ASTM D-2794</i>)	35.43	53.15	70.86
Pencil hardness (<i>ASTM D-3363</i>)	H	2H	3H
Abrasion Resistance (weight loss in mg, CS-17 and 1Kg) (<i>ASTM D-4060</i>)			
500 cycles	63.4	49.9	37.3
1000 cycles	Film removed	78.3	57.7
Chemical Resistance			
5% HCl	Passes	Passes	Passes
5% NaOH, (Rating as per ASTM D-714)	Medium dense blisters (Size no. 6)	Medium blisters (Size no. 6)	Few blisters (Size no. 4)

Abrasion resistance was observed to follow the similar trend as that of pencil hardness when evaluated using a CS-17 wheel under 1 Kg load for various cycles (500 and 1000 cycles). The increased surface hardness of HC_50 formulation due to increased siloxane linkages was responsible for its better abrasion resistance compared to the others. The increased cross-link density in the coatings was balanced by the soft oligomeric segment of hybrid sol, which did not result in any brittleness of the coatings. Hence the abrasion resistance was observed to improve as the percentage of hybrid sol was increased to 50% (i.e., HC_50). Table 1 shows the results obtained for all the mechanical properties for all coating samples evaluated.

5.2.3 Chemical Resistance Properties

The chemical resistance of the coatings was evaluated for acid and alkali resistance. The coated substrates were dipped in 5% NaOH and 5% HCl solution respectively for 12 hours. After completion of test, panels were inspected for visible damages, if any. All the formulations showed excellent acid resistance. However, few to medium-dense blistering was observed in the case of alkali resistance as evaluated from HC_50 to HC_0 respectively, which could be due to the presence of ester linkages in the polymeric network which are susceptible to hydrolysis in an

alkaline environment. The increased number of siloxane linkages in HC_50 help to suppress the effect of chemical penetration across the film, thereby imparting comparatively good resistance irrespective of ester linkages present in the film. The degree of blistering was evaluated and reported as per ASTM D 714-02.

5.2.4 Solvent Resistance Properties

The film integrity of the coated panels was evaluated in polar (methanol) and non-polar (xylene) solvent by immersion method. After 4 hrs of immersion, visible examination of the coated panel shows no blister or pit formation on the coated surface. All the coatings showed excellent solvent resistance for both methanol and xylene. The exposed area was further evaluated for secondary adhesion and it was observed to be 5B for all formulations.

5.2.5 Hydrolytic Stability

After completion of 4 hr immersion in boiling water, the panels were dried and observed for any film defects, if any. The coating HC_50 showed superior hydrolytic stability compared to HC_0 (neat) and HC_30 formulation. This could be due to increased silane content resulting in increased Si-O-C linkages,

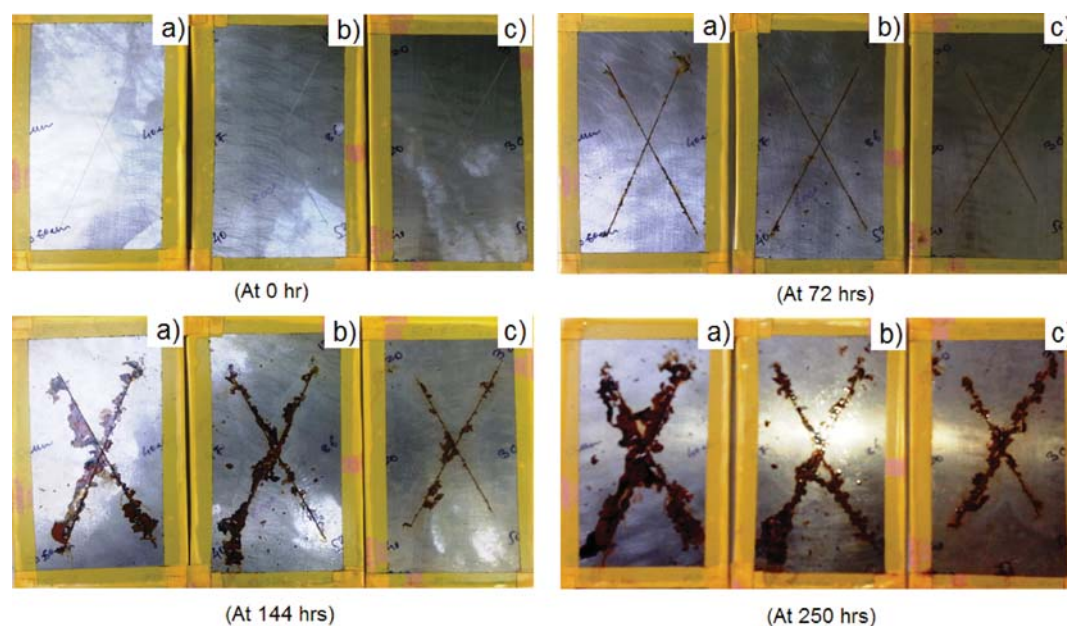


Figure 8 Salt spray images of (a) HC_0 (neat), (b) HC_30 and (c) HC_50 coatings after 0, 72, 144 and 250 hrs of exposure in 3.5% NaCl solution.

which are hydrolytically more stable. The strong siloxane linkages (-Si-O-Si-) formed after condensation between TEOS and GPTMS would also contribute to excellent hydrolytic stability. The secondary adhesion of coatings was also evaluated, which was observed to be unaffected for HC_50 formulation. The test results revealed the zero water permeability of HC_50 film. However, few blisterings were observed in HC_0 (neat) and HC_30 formulation. The results were reported as per ASTM D 714-02.

5.2.6 Anti-Corrosive Properties

The corrosion resistance properties of all the coating systems were evaluated by exposing the coated panels to 3.5 wt% aqueous sodium chloride (NaCl) solution at 35 ± 2 °C according to ASTM B-117 specifications. The appearance of the coated panels after 0, 72, 144 and 250 hrs of salt spray test is shown in Figure 8. It can be identified that rusting was started after 72 hrs due to metal exposure to electrolytic chemical (3.5% NaCl). The degree of rusting across the scribed area was observed to be extended in neat (HC_0) and formulation HC_30 after 144 hrs and 250 hrs of exposure, as shown in Figure 8. However, HC_50 formulation shows comparatively lesser corrosion across the scribed area, which indicates that the adhesive forces between coating and metal substrate increase significantly on increasing the content of hybrid precursor. The improved adhesion and increased number of siloxane linkages (-Si-O-Si-) on increasing the content of hybrid sol helps to impede the penetration of water and chloride ions (Cl⁻ ions)

across the scribe, hence preventing the propagation of corrosion at metal coating interface.

Table 1 shows secondary adhesion of all the coatings after 250 hrs of salt spray test. The adhesion was observed to be decreased with value of 4B and 3B for HC_30 and HC_0 formulations respectively, while it was unaffected (5B) for HC_50 formulation.

5.2.7 Electrochemical Properties

Electrochemical impedance spectroscopy (EIS) was used to evaluate the anti-corrosive performance of the coatings. From the polarization curves (Figure 9) in the 3.5% NaCl solution, it can be seen that the corrosion current for the HC_0 formulation is larger than that of the other formulations. The incorporation of MCHP resulted in lower current densities which showed a continuous decreasing trend with further increase in the content of hybrid precursor. The decreased I_{corr} (μA) values and corrosion rate (mm/yr) (as shown in Table 2) with increasing CNSL-based hybrid precursor (MCHP) indicated that more siloxane as well as metallo siloxane linkages indeed could provide a physical barrier for blocking the electrochemical process at metal coating interface, as also indicated by FTIR study.

Figure 10 shows a typical Bode plot for all the formulations. Generally, higher Z modulus at lower frequency indicates a better corrosion resistant coating on the metal substrate [31]. The Bode plot shows higher Z modulus values in the order of $10^8 \Omega$ at lower frequency for HC_50 compared to $10^7 \Omega$ and $10^6 \Omega$

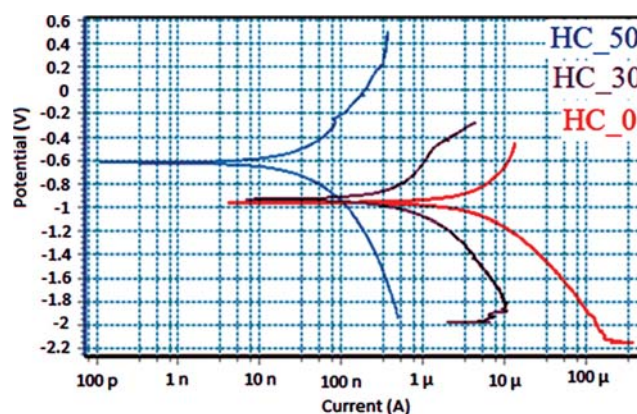


Figure 9 Potentiodynamic polarization curves of HC_0 (neat), HC_30 and HC_50 coatings in 3.5% NaCl.

Table 2 Electrochemical parameters for CNSL-based hybrid coatings on Mild steel in 3.5% NaCl solution.

Formulation	I _{corr} (μA)	E _{corr} (mV)	Corrosion Rate (mm/yr)	Impedance (Ω)
HC_0	2.18×10^{-9}	-0.982	5.56×10^{-3}	9.2345×10^6
HC_30	4.29×10^{-10}	-0.954	3.71×10^{-5}	2.569×10^7
HC_50	8.13×10^{-12}	-0.598	1.15×10^{-6}	1.8734×10^8

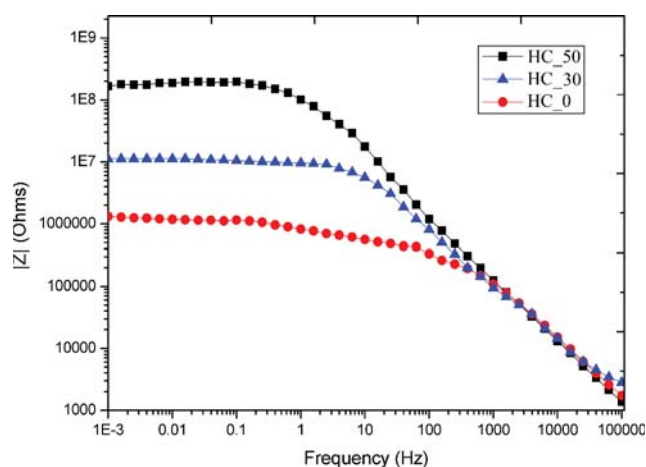


Figure 10 Bode plots of HC_0 (neat), HC_30 and HC_50 coatings in 3.5% NaCl.

for HC_30 and HC_0 formulations respectively. This further suggests that the level of porosity and defects present in the developed coatings is very low, which helps to explain the excellent corrosion protection.

5.2.8 UV Resistance Properties

The UV resistance of the coated specimen was evaluated by exposing the coated panels to alternate 4 hr cycles of UV light and water condensation for 360 hrs (Figure is given in supporting information). Damage caused by the weathering cycle was assessed using

visual assessment, gloss measurement and color values (L, a, b values). Table 3 shows Yellowness index, Lab values and % variation in ΔE of all the coatings at 0 hrs and 360 hrs.

It was observed that the addition of MCHP in the conventional Alkyd-MF coating system improves the weatherability property of the coatings. Also, the % variation in Yellowness index and ΔE was observed to be decreased on increasing the content of hybrid precursor (MCHP). This could be attributed to a greater number of siloxane linkages in the HC_50 formulation. The increased number of stronger Si-O

Table 3 Color properties before and after 360 hrs of UV exposure with alternate condensation cycles.

Formulation	Yellowness Index (YI) (ASTM D-1925)	Variation in YI	L*	a*	b*	% variation in ΔE
HC_0						
0 hrs	1.624	28.53	65.655	0.316	0.527	54.2%
360 hrs	47.965		50.084	3.286	15.733	
HC_30						
0 hrs	8.036	2.422	63.604	0.006	3.045	11.28%
360 hrs	27.531		61.137	-1.462	10.907	
HC_50						
0 hrs	19.671	0.37	60.345	-0.102	7.622	3.15%
360 hrs	27.404		59.756	-1.235	11.465	

bonds (bond dissociation energy of 190.73 Kcal/mol) in HC_50 formulation imparted the enhanced UV resistance as that of other formulations. The visual examination of the exposed specimen shows that HC_50 formulation showed excellent resistance against formation of corrosion products (pits) on the surface after UV exposure. The gloss retention of the HC_50 formulation was observed to be 75.26% after 360 hrs. The gloss retention values of neat and 30% formulation were unable to be measured due to the formation of pits on the surface after exposure.

5.2.8 SEM/EDAX Analysis

The surface morphology of all the coating systems was evaluated by scanning electron microscope using Quanta 200 SEM instrument (FEI Company, USA). The SEM micrographs revealed that the coating on mild steel is uniform, homogenous, and crack free. The EDAX graphs shows uniformly distributed silica with an increase in area under the peak at 1.79 keV (Figure is given in supporting information) for HC_50 compared to HC_30. This confirmed the presence of increased silica on increasing the content of MCHP.

6 CONCLUSION

A renewable resource-based sustainable coating system was successfully developed by partially replacing conventional hardener with newly synthesized CNSL-based hybrid precursor in conventional stoving systems; and their performance in terms of mechanical properties, chemical resistance, solvent resistance and hydrolytic stability and accelerated weathering were evaluated. All mechanical properties were observed to be similar for all the coatings except the increasing trend in pencil hardness with increasing MCHP content, which could be due to increased

crosslinking density. The formulation containing 50% of CNSL-based hybrid precursor (HC_50) showed excellent performance in terms of chemical and solvent resistance properties. Silicone modification increased the corrosion resistance and UV stability of the system. Improvement in corrosion resistance is attributed to the formation of more siloxane linkages (Si-O-Si) at metal-coating interface, which are quite stable in an aggressive environment. Furthermore, the combination of long-chain methylene linkages of CNSL and the presence of siloxane (Si-O-Si) moieties after GPTMS modification in the coatings maintained a good balance between flexibility and hardness of the coating. Thus, this CNSL, natural resource, can be used as one of the potential alternatives to some of the petroleum-based raw materials, and can be accepted as an eco-friendly coating system with increased performance properties.

Acknowledgments

The authors gratefully acknowledge Cardolite Corporation, Mangalore, and Shalimar Paints Ltd., Nashik, for their kind support in supplying raw materials and testing facilities respectively. The author would also like to thank Dr. Swapan K. Ghosh – Director of Nova Surface-Care Centre, India – for his fruitful discussion and kind support in terms of testing facilities in his lab.

REFERENCES

1. U.S. Department of Health and Human Services, Public Health Service, Agency for Toxic Substances and Disease Registry, www.atsdr.cdc.gov/toxprofiles/tp7.pdf (2008).
2. U.S. Environmental Protection Agency, Washington, DC, <http://www.epa.gov/iris/toxreviews/0144tr.pdf> (1998).

3. F. Zafar, S.M. Ashraf, and S. Ahmad, Air drying polyesteramide from a sustainable resource. *Prog. Org. Coat.* **51**, 250–256 (2004).
4. X. Pan, P. Sengupta, and D.C. Webster, High bio-based content epoxy-anhydride thermosets from epoxidized sucrose esters of fatty acids. *Biomacromolecules* **12**, 2416–2428 (2011).
5. C.B. Ferrer, E. Hablot, M.C. Garrigos, S. Bocchini, L. Averous, and A. Jimenez, Relationship between morphology, properties and degradation parameters of novative bio-based thermoplastic polyurethanes obtained from dimer fatty acids. *Polym. Degrad. Stab.* **97**, 1964–1969 (2012).
6. W.D. Oliveira and W.G. Glasser, Multiphase materials with lignin. II. Starlike copolymers with caprolactone. *Macromolecules* **27**, 5–11 (1994).
7. Y. Li, J. Mlynar, and S. Sarkanen, The first 85% kraft lignin-based thermoplastics. *J. Polym. Sci. B Polym. Phys.* **35**, 1899–1910 (1997).
8. N. Cordeiro, P. Aurenty, M.N. Belgacem, A. Gandini, and C.P. Neto, Surface Properties of Suberin. *J. Colloid Interface Sci.* **187**, 498–508 (1997).
9. M.J. Dumont, X. Kong, and S.S. Narine, Polyurethanes from benzene polyols synthesized from vegetable oils: Dependence of physical properties on structure. *J. Appl. Polym. Sci.* **117**, 3196–3203 (2010).
10. A.K. Mohanty, M. Misra, and G. Hinrichsen, Biofibres, biodegradable polymers and biocomposites: An overview. *Macromol. Mater. Eng.* **276/277**, 1–24 (2000).
11. D.G. Barrett, T.J. Merkel, L.J. Christopher, and M.N. Yousaf, One-step syntheses of photocurable polyesters based on a renewable resource. *Macromolecules* **43**, 9660–9667 (2010).
12. G.C. Ayli and S.K. Usefoglul, Biobased polyisocyanates from plant oil triglycerides: Synthesis, polymerization, and characterization. *J. Appl. Polym. Sci.* **109**, 2948–2955 (2008).
13. S. Ma, X. Liu, Y. Jiang, Z. Tang, C. Zhang, and J. Zhu, Bio-based epoxy resin from itaconic acid and its thermosets cured with anhydride and co-monomers. *Green Chem.* **15**, 245–254 (2013).
14. D. Juais, F.N. Alliny, C. Li, and A.G. Richard, Isosorbide polyesters from enzymatic catalysis. *Macromolecules* **43**, 10315–10319 (2010).
15. D. Feldman, M. Lacasse, and M.R. St. John, Polyurethane-based sealants modified by blending with Kraft lignin. *J. Appl. Polym. Sci.* **35**, 247–257 (1988).
16. D. Balgude and A. Sabnis, CNSL: An environment friendly alternative for the modern coating industry. *J. Coat. Technol. Res.* **11**, 169–183 (2014).
17. B. Wesseling, Passivation of metals by coating with polyaniline—Corrosion potential shift and morphological changes. *Adv. Mater.* **3**, 226–228 (1994).
18. N. Ahmad and A.G. MacDiarmid, Inhibition of corrosion of steels with the exploitation of conducting polymers. *Synth. Met.* **78**, 103–110 (1996).
19. M. Yoshida and J. Lahann, Smart nanomaterials. *ACS nano* **2**, 1101–1107 (2008).
20. D. Wang and G.P. Bierwagen, Sol-gel coatings on metals for corrosion protection. *Prog. Org. Coat.* **64**, 327–338 (2009).
21. D. Balgude and A. Sabnis, Sol-gel derived hybrid coatings as an environment friendly surface treatment for corrosion protection of metals and their alloys. *J. Sol-Gel Sci. Technol.* **64**, 124–134 (2012).
22. Y. Nakayama, Maleinization process, US Patent 3778418, assigned to Kuraray Co., Ltd. (December 11, 1973).
23. M. Kathalewar and A. Sabnis, Epoxy resin from cardanol as partial replacement of bisphenol-A-based epoxy for coating application. *J. Coat. Technol. Res.* **11**, 601–618 (2014).
24. A.N. Khramov, V.N. Balbyshev, N.N. Voevodin, and M.S. Donley, Nano-structured sol-gel derived conversion coatings based on epoxy- and amino-silanes. *Prog. Org. Coat.* **47**, 207–213 (2003).
25. D.L. Pavia, G.M. Lampman, G.S. Kriza, and J.R. Vyvyan, *Introduction to Spectroscopy*, pp. 28–29, Brooks/Cole, Cengage Learning Inc., United States. (2009).
26. G.R. Rossman, Vibrational Spectroscopy of Hydrous Components. In: FC Hawthorne, ed., *Spectroscopic Methods in Mineralogy*. *Rev. Mineral.* **18**, 193–206 (1988).
27. C. Li and C.L. Wilkes, Silicone/amine resin hybrid materials as abrasion resistant coatings. *Chem. Mater.* **13**, 3663–3668 (2001).
28. G. Gupta, S.S. Pathak, and A.S. Khanna, Anticorrosion performance of eco-friendly silane primer for coil coating applications. *Prog. Org. Coat.* **74**, 106–114 (2012).
29. R.M. Silverstein, F.X. Webster, and D.J. Kiemle, *Spectrometric Identification of Organic Compounds*, pp. 127–227, John Wiley & Sons, Inc., United States. (2005).
30. R.H. Glaser, G.L. Wilkes, and C.E. Bronnimann, Solid-state ²⁹Si NMR of TEOS-based multifunctional sol-gel materials. *J. Non-Cryst. Solids* **113**, 73–87 (1989).
31. M. Kathalewar, A. Sabnis and G. Waghoo, Effect of incorporation of surface treated zinc oxide on non-isocyanate polyurethane based nano-composite coatings. *Prog. Org. Coat.* **76**, 1215–1229 (2013).